TÜBİTAK

Turkish J. Eng. Env. Sci.
35 (2011) , 139 – 158.

doi:10.3906/muh-1102-5

A method for optimum cavitating ship propellers

Şakir BAL
İstanbul Technical University, Department of Naval Architecture and Marine Engineering
Maslak, Sarıyer, İstanbul, 34469, TURKEY
e-mail: sbal@itu.edu.tr

Received: 16.02.2011

Abstract

A practical design method was applied to obtain optimum cavitating ship propellers by combining a vortex lattice lifting line method (propeller design program) and a lifting surface method (propeller analysis program). The optimum circulation distribution that gives the maximum lift-to-torque ratio was computed for given thrust and given chord lengths along the radius of the propeller by a vortex lattice solution to the lifting line problem. The section details of the blades, such as pitch-to-diameter ratio and camber ratio, were then found to obtain the desired (optimal) circulation distribution automatically by a lifting surface method. In order to get the optimum circulation distribution, the radius of the blades was divided into a number of panels extending from hub to tip. The radial distribution of bound circulation could be computed by a set of vortex elements that have constant strengths. A discrete trailing free vortex line was shed at each of the panel boundaries with strength equal to the difference in strengths of the adjacent bound vortices. The vortex system was built from a set of horseshoe vortex elements, each consisting of a bound vortex segment of constant strengths and 2 free vortex lines of constant strengths. An algebraic equation system could be formed by using these vortex systems. Once this equation system for unknown vortex strengths was solved with a specified thrust, the optimum circulation distribution and the forces could be computed by the Betz-Lerbs method. When the radial distribution of optimum circulation and chord length were reached, the lifting surface method could be applied to determine the blade pitch and camber in order to produce the desired circulation automatically. The lifting surface method also accounts for cavitation, which is an avoidable physical phenomenon on the blades. The cavity effects in the present method were represented by using cavity sources and cavitating velocities, which were evaluated on the blade surface beneath the cavity. The practical design technique was applied both to noncavitating and cavitating DTMB 4119 and DTMB 4381 propellers, for which the hydrodynamic characteristics are given in the literature, and the results were compared with those given in the literature. A very good level of satisfaction was obtained for practical applications.

Key Words: Optimum ship propeller, cavitation, propeller design, propeller analysis, vortex lattice method, lifting surface method, lifting line method

1. Introduction

A cavitating ship propeller that has the highest propeller coefficient (i.e. maximum thrust-to-torque ratio) is known as optimum in terms of hydrodynamic performance. The objective of ship propeller design is to obtain the highest efficiency subject to prescribed requirements from a hydrodynamic point of view. On the other hand, cavitation, which is an avoidable physical phenomenon, has always been a major concern in propeller design. Sheet cavitation is especially very common in ship propellers, as explained by Kerwin (1986) and Kinnas et al. (2005). A reliable and effective numerical technique including sheet cavitation is thus very crucial for the design of ship propellers. This paper addresses the computation of pitch, chord length, and camber distribution along the radius of an optimum cavitating propeller in steady flow by combining a vortex lattice method and a lifting surface method. The effects of skew and rake on the optimum cavitating propeller were, however, ignored in this stage of the present study.

Cavitation occurs when the pressure is below the vapor pressure of fluid, and its presence can lead to propeller erosion and noise. The periodic occurrence and collapse of cavities due to an unsteady, nonaxisymmetric inflow also leads to periodic pressure fluctuations and can cause vibrations of the hull and the shaft, which may lead to fatigue and failure of these structures. In the past, a propeller was designed in a way such that cavitation was completely avoided. Although such methods have been well applied to lightly loaded propellers, the application to heavily loaded and/or high-speed propellers is not appropriate, since cavitation is much more likely to occur in these conditions. Additionally, the efficiency of a cavitating blade may be higher than that of a noncavitating blade because of less frictional loss at the parts of the blade that are covered by sheet cavitation. The present work addresses the simulation of sheet cavitation, which forms on the propeller blade's surface and remains attached to it like a thin vapor bubble. Studies on sheet cavitation are important because sheet cavity is a very common type of cavity on ship propellers and can affect both the radiated pressure field and the formation of cloud cavitation.

2. Previous works

Many researchers and engineers have contributed to the improvement of cavitating propeller design. Kerwin (2001) stated that the actuator disk was one of the earliest and simplest theories for propeller analysis and is the limit case of a propeller with the highest efficiency at a specified thrust. It corresponds to the case of no hub with an infinite number of blades and an infinitesimally small advance coefficient and chord lengths. Betz (1919), on the other hand, first developed the basis for determining the radial distribution of circulation that would result in maximum efficiency for a propeller in uniform inflow. He analyzed the trailing vortex wake far downstream of the propeller and found the "Betz condition," stating that the induced inflow on the lifting line must have a radial constant pitch. However, the propeller design problem was actually solved by Goldstein (1929). He developed a propeller design method following Prandtl's lifting line concept. He obtained the "Goldstein circulation reduction factor," the ratio of circumferential mean tangential induced velocity and the local tangential induced velocity at the lifting line. The extension of Goldstein's lifting line theory to the case of propellers with arbitrary radial distributions of circulation in both uniform and radial varying axisymmetric inflow was presented by Lerbs (1952), who derived the "Lerbs criteria" for optimum propellers. The optimum circulation distribution on a propeller with a duct of finite length was determined by Sparenberg (1969). He discussed the effects of tip clearances and hub diameter. A vortex lattice method to analyze and design a marine propeller was used by Kerwin and Lee (1978) and Greely and Kerwin (1982), respectively. The

continuous singularities on the lifting surfaces (blades) were represented by a set of vortex/source lattices. The blade loading and vorticity in the trailing wake were represented by vortex lattices distributed on the mean camber surface while the blade thickness was accounted for by adding thickness source panels. A review of the hydrodynamic aspects of marine propellers up to the middle of the 1980s was published by Kerwin (1986). An extensive overview of the hydrodynamics of ship propellers was presented by Breslin and Andersen (1994).

Coney (1992) later developed a design method for the optimal circulation distribution based on variational optimization. He represented the propeller by concentrated lifting lines (horseshoe vortex elements) and described the thrust and torque as functions of horseshoe strengths that were solved for constrained optimization. The method was applicable to multicomponent propulsors, such as ducted propellers and propeller-stator combinations. An unsteady propeller design method, which intended to optimize the cavitation inception speed, was developed by Kuiper and Jessup (1993). They focused on blade section design. An artificial intelligence for the preliminary propeller design was used by Dai et al. (1994). They discussed the numerical optimization and genetic algorithms. Mishima and Kinnas (1997) developed a numerical method to determine the blade geometry with the best efficiency for specified thrust and cavity size constraints. The propeller performance was described as a function of design variables whose combination determined the blade geometry. The unsteady propeller analysis algorithm was coupled with a constrained nonlinear optimization algorithm. Griffin and Kinnas (1998) further improved the propeller analysis and design methods. In particular, the analysis method was improved in such a way that the cavity search algorithm was included along the blade section. The design method was also extended to include the skew distribution and minimum pressure constraint. The coupled axisymmetric RANS calculation and vortex/source lattice method were later applied by Kerwin et al. (2003) to the design of ducted propellers. Further analysis and design techniques for ducted propulsors and viscous/inviscid interaction can be found in the works of Kinnas et al. (2005) and Sun (2008), respectively.

3. Present work

In the present study, the hydrodynamic design of a cavitating ship propeller was carried out in 2 steps. First, a lifting line model was used to determine the optimum radial distribution of circulation over the blades to produce the desired thrust with the highest propeller efficiency. Second, the shape of the blades (chord, pitch, and camber distributions) required to produce this desired distribution of circulation was determined. The effects of skew and rake were not considered in this stage of the present study. The propeller vortex lattice solution (PVL; code given by Kerwin (2001)) to the lifting line problem of the propeller, in which the blades are considered to have concentrated lines of bound vortices, was used to predict the optimum circulation distribution over the blades in this study. However, the lifting line theory cannot alone provide the actual blade geometry that produces the desired circulation distribution. A more elaborate representation of the propeller should be employed to determine the blade pitch, chord, and camber distribution in order to produce the desired circulation over the blade. A lifting surface method, very similar to the one applied to the podded propulsors presented by Bal and Güner (2009), was used here for this purpose. The blades were modeled as sheets of vortex/source singularities with unknown strengths. The lifting surface method accounts for cavitation characteristics of the blades by using cavity source singularities. The strengths of singularities can then be found by applying the appropriate boundary conditions on the blades and cavity surfaces. The steady loading as well as the unsteady forces and cavity patterns on the blades can be predicted by this lifting surface method. In the following sections, the design and analysis methods of the propeller are explained and these methods are applied to a DTMB 4119

propeller, working both at noncavitating and cavitating conditions, and to a DTMB 481 propeller, and the results are compared with those given in the literature.

4. Propeller design method

The lifting line theory was employed here to represent the propeller as a set of a number of blades (NB) and straight and radial lifting lines. The lifting lines represent blades of the propeller. The blades have angular spacing and equal loading. The geometry (i.e. pitch, camber, and chord) of the actual propeller is replaced by a radial distribution of circulation. The lifting lines rotate with angular velocity ω around the x-axis. The lifting line starts at hub radius r_h and extends to propeller radius R. A cylindrical coordinate system (x, r, θ) is assumed to be rotating with the propeller. Refer to Kerwin (2001) for details.

The strength of bound vortices on the blades is the circulation distribution over the blades, $\Gamma(\mathrm{r})$. The shape of the free vortex wake is, however, assumed to be helical. Under the linear lifting line method, the pitch ($\beta(\mathrm{r})$) of the helixes can be determined by the propeller's rotation and undisturbed inflow:

$$\beta(r) = \tan^{-1}\left[\frac{V_a(r)}{\omega r + V_t(r)}\right], \tag{1}$$

where $\mathrm{V}_a(\mathrm{r})$ is an effective axial inflow and $\mathrm{V}_t(\mathrm{r})$ is an effective tangential inflow for each radius over the blades. The shape of the helixes can also be aligned with the induced velocities at the lifting line. For a propeller with optimum radial load distribution according to the Betz (1919) condition, the efficiency for each blade section should be constant and equal to (see also Kerwin (2001)):

$$\frac{\tan\beta(r)}{\tan\beta_i(r)} = constant. \tag{2}$$

Here, β_i is the hydrodynamic pitch angle and can be given as:

$$\beta_i(r) = \tan^{-1}\left[\frac{V_a(r) + u_a^*(r)}{\omega r + V_t(r)}\right], \tag{3}$$

where $u_a^*(r)$is the axial induced velocity due to the helical free vortex system. Similarly, the Betz condition can be extended to the case of nonuniform axial inflow according to the Lerbs (1952) condition:

$$\frac{\tan\beta(r)}{\tan\beta_i(r)} = \gamma\sqrt{1 - w_x(r)}. \tag{4}$$

Here, $\mathrm{w}_x(\mathrm{r}) = 1 - [\mathrm{V}_a(\mathrm{r}) \,/\, \mathrm{V}_s]$, V_s is the ship speed, and γ is an unknown constant.

Expressions for the forces acting on radius r on the lifting line can be developed from a local application of the Kutta-Joukowski theorem. These forces can then be resolved into components in the axial and tangential direction, integrated over the radius, and summed over the number of blades to produce the total propeller thrust and torque values. Refer to Kerwin (2001) for details about the lifting line theory of propellers.

5. The vortex lattice solution to the lifting line problem

The continuous distribution of vortices along the lifting line is discretized by vortex lattice elements with constant strengths. The element arrangement along the lifting line employs both uniform spacing and cosine

spacing. The induced velocity is calculated at control points located at the mid-radius of each panel. Thus, the radius of each lifting line is divided into M panels of length Δr and the continuous distribution of circulation over the radius can be replaced by a step-like distribution. The value of the circulation in each panel, Γ(i), is set equal to the value of the continuous distribution at the control points. Since the circulation is piecewise constant, the helical free wake vortex sheet is replaced by a set of concentrated, helical vortex lines shed from each panel boundary. The strength of these trailing vortices is equal to the difference in bound vortex strength across the boundary. Therefore, it can be considered that the continuous vortex distribution is to be replaced by a set of vortex horseshoes. Each of these horseshoes consists of a bound vortex filament and 2 helical trailing vortices.

The velocity induced at the lifting line by this system of vortices can be computed using the very efficient formulas given by Kerwin (2001). They are not repeated here. The velocity induced at a given point is a summation of the velocities induced by each vortex horseshoe:

$$u_a^*\left(r(i)\right) \equiv u_a^*(i) = \sum_{m=1}^{M} \Gamma(m)\bar{u}_a^*(i,m), \tag{5}$$

$$u_t^*\left(r(i)\right) \equiv u_t^*(i) = \sum_{m=1}^{M} \Gamma(m)\bar{u}_t^*(i,m), \tag{6}$$

where u_a^* and u_t^* are the axial and tangential components of induced velocity. $\bar{u}_a^*$ and $\bar{u}_t^*$ are the axial and tangential components of induced velocity at the control point at radius r(i) by a unit, the helical horseshoe vortex surrounding the control point at r(m). Under this discrete model, the integrations for the total forces are replaced by the summations over the number of panels. The PVL code is based on this method and uses the Betz-Lerbs condition to obtain the optimum circulation distribution over blades. Here it was used to get the optimum circulation distribution (i.e. maximum thrust-to-torque ratio) for a given thrust. Refer to Kerwin (2001) for details of the vortex lattice solution to the lifting line model and PVL code.

6. Propeller analysis method

A lifting surface method was developed and used to calculate the propulsive performance and induced velocities due to the propeller, similar to the one given by Bal and Güner (2009). The lifting surface method (propeller analysis code) models the 3-dimensional unsteady cavitating flow around a propeller by representing the blade and wake as a discrete set of vortices and sources, which are conveniently located on the blade mean camber surface and wake surface. In particular, the 3 components of the discretization are as follows:

i) A vortex lattice on the blade mean camber surface and wake surface to represent the blade loading and trailing vorticity in the wake.

ii) A source lattice on the blade mean camber surface to represent blade thickness.

iii) A source lattice throughout the cavity extent to represent cavity thickness.

The sources representing blade thickness are line sources along the spanwise direction. The strengths of the line sources are given in terms of derivatives of the thickness in the chordwise direction and are independent

of time as presented by Griffin and Kinnas (1998). The unknown bound vortices on the blade and the unknown cavity sources are determined by applying the kinematic boundary condition and the dynamic boundary condition. The kinematic boundary condition is given as:

$$\frac{\partial \phi}{\partial n} = -\vec{U}_{in}.\vec{n}, \tag{7}$$

where $\vec{n}$ is the surface unit normal vector to the mean camber blade surface at the kinematic boundary condition control point, $\vec{U}_{in}$ is the inflow velocity with respect to the propeller-fixed coordinate system, and ϕ is the perturbation potential. In this method, a discretized version of the kinematic boundary condition is employed as:

$$\sum_{\Gamma} \Gamma \, \vec{v}_{\Gamma} \cdot \vec{n}_m = -\vec{v}_{in} \cdot \vec{n}_m - \sum_{Q_B} Q_B \, \vec{v}_Q \cdot \vec{n}_m - \sum_{Q_C} Q_C \, \vec{v}_Q \cdot \vec{n}_m, \tag{8}$$

where $\vec{v}_{\Gamma}$ is the velocity vector induced by each unit strength vortex element, $\vec{v}_Q$ is the velocity vector induced by each unit strength source element, and $\vec{n}_m$ is the unit vector normal to the mean camber line or trailing wake surface. Q_B and Q_C represent the magnitude of the line sources that model the blade thickness and cavity source strengths, respectively. The kinematic boundary condition must be satisfied at certain control points located on the blade mean camber surface. The kinematic boundary condition requires that the sum of the influences for all of the vortices' sources and the inflow normal to a particular control point on the blade is equal to zero. Another way to explain this is that the kinematic boundary condition requires the flow to be tangential to the surface. The dynamic boundary condition is based on Bernoulli's equation between a point far from the propeller and the point of interest. This condition is defined as given by Griffin and Kinnas (1998):

$$p - p_{shaft} = -\rho \frac{\partial \phi}{\partial t} - \rho u V_r - \rho g y_s, \tag{9}$$

where p is the pressure at the point of interest, p_{shaft} is the pressure at a point far from the propeller at the depth of the shaft axis, ρ is the density of water, $\frac{\partial \phi}{\partial t}$ is the time derivative of the potential induced by all of the singularities, u is the perturbation velocity along the chordwise direction, V_r is the unperturbed velocity with respect to the propeller system, and y_s is the hydrostatic depth of the point of interest.

The dynamic boundary condition requires that the pressure must be equal to vapor pressure at control points covered by the cavity. The area of application of the dynamic boundary condition changes with time as the cavity extent changes with time. The unknown cavity extent is determined by searching for the cavity length along each spanwise location. The desired cavity length is the one that renders the cavity pressure equal to vapor pressure. The pressures on the cavity and blade are evaluated via Bernoulli's equation with the 3-dimensional linearized velocity terms, the unsteady terms $\frac{\partial \phi}{\partial t}$, and the hydrostatic terms fully included. The cavity thickness (and thus volume) is determined by integrating the cavity source distribution over the cavity surface along each strip. The problem is solved in the time domain with each time step representing an angular rotation of the propeller. The time domain solution allows for the effects of all strips and blades to be accounted for in an iterative fashion. After the first complete propeller revolution, the method achieves the fully wetted steady solution, and 3 more propeller revolutions produce the fully wetted unsteady solution. Finally, the cavitating unsteady solution is attained after a total of 7 or more propeller revolutions. Refer to Griffin and Kinnas (2001) for details.

Other assumptions employed throughout the method include:

i) The cavity thickness varies linearly across panels in the chordwise direction and is piecewise constant across panels in the spanwise direction.

ii) There are no spanwise flow effects in the cavity closure condition.

iii) Viscous force is calculated by applying a uniform frictional drag coefficient, C_f, on the wetted regions of the blade.

The induced velocities due to vortex elements of the lifting surface are calculated using the Biot-Savart law, expressed as:

$$\overrightarrow{V}_\Gamma = \frac{\Gamma}{4\pi}.\frac{\vec{L}x\vec{d}}{\vec{d}^3}, \tag{10}$$

where $\overrightarrow{V}_\Gamma$ is induced velocity, Γ is circulation, $\vec{L}$ is the vortex length element, and $\vec{d}$ is the distance between the element and the field point. The induced velocities due to sources/sinks are also computed on the basis of given source/sink intensity. Once the bound vortex elements' intensity is solved, then the velocity induced by the propeller in any point in space can be computed using angular positions of the propeller blade. The forces on the propeller blade are found by the Kutta-Joukowski theorem. The contributions of all lattice elements to the total forces are added along the blades. If the propeller is working in a steady state condition, the forces on all blades are the same. Hence, the force on the entire propeller is found by multiplying each blade force by the number of blades. Hub effect, using the method of images, can also be included into the calculations. Refer to Kerwin (2001), Griffin and Kinnas (1998), and Bal and Güner (2009) for details of the lifting surface method of solution to the propeller analysis problem.

7. Combining propeller design and analysis methods

The steps of hydrodynamic design of a cavitating ship propeller can be simply accomplished as follows:

1. First, the radial distribution of circulation over the blades that will produce the required total thrust with maximum efficiency is established using a propeller design method (PVL code) for a given chord distribution. The radial distribution of chord length is a necessary input to the viscous force calculations of the circulation optimization. In order to minimize viscous drag forces, it is desirable to keep the propeller chord length as short as possible. However, the strength considerations limit how short these chord lengths may become. The selection of these quantities, however, is not discussed in this stage of the present study. It is assumed that the initial chord length distribution is taken from original propellers and kept fixed during the calculations.

2. The actual shape of the blade (pitch and camber distribution over the blade) that will produce this prescribed distribution of circulation can then be developed using the propeller analysis method (lifting surface solution) automatically. In order to do this, a code that calls the propeller analysis method (lifting surface solution) repeatedly is developed. This code changes automatically, in a systematic way, the pitch distribution and camber distribution to produce the desired (optimum) circulation distribution for given chord lengths over the blades. The code runs very fast and includes cavity patterns. It should, however, be noted that the number of blades and the chord distribution can be changed to produce the required thrust value and to minimize the cavity formation.

8. Validation and numerical results

8.1. Noncavitating DTMB 4119 propeller

The lifting surface method for validation was first applied to a noncavitating DTMB 4119 propeller. The DTMB 4119 propeller has the following geometric characteristics and working conditions (refer to Brizzolara et al. (2008) for details):

i) The propeller inflow is uniform.

ii) The propeller has 3 blades, i.e. NB = 3.

iii) The hub-to-diameter ratio is 0.2.

iv) The blade geometries from reference in terms of radial distribution of the chord length (c), camber (f), thickness (t), and pitch (P) are shown in Table 1.

v) The blade sections are designed with NACA 66 modified profiles and a camber line of a = 0.8. Refer to Abbott and Doenhoff (1959).

vi) The propeller has no skew and no rake.

Table 1. DTMB 4119 propeller geometry taken from Brizzolara et al. (2008).

r/R	c/D	P/D	t_{max}/c	f_{max}/c
0.20	0.3200	1.1050	0.2055	0.0143
0.30	0.3635	1.1022	0.1553	0.0232
0.40	0.4048	1.0983	0.1180	0.0230
0.50	0.4392	1.0932	0.0902	0.0218
0.60	0.4610	1.0879	0.0696	0.0207
0.70	0.4622	1.0839	0.0542	0.0200
0.80	0.4347	1.0811	0.0421	0.0197
0.90	0.3613	1.0785	0.0332	0.0182
0.95	0.2775	1.0770	0.0323	0.0163
0.98	0.2045	1.0761	0.0321	0.0145
1.00	0.0800	1.0750	0.0316	0.0118

The lifting surface analysis program was run for the propeller under the above conditions. There were 20 vortex lattices (N = 20) used along the chordwise direction and 18 vortex lattices (M = 18) used along the radius of the blades. The frictional drag coefficient $C_f = 0.004$ was used in the calculations. The perspective view of the DTMB 4119 propeller with its wakes and the vortex elements used in the lifting surface analysis program are shown in Figures 1 and 2, respectively. The thrust and torque coefficients (K_T and K_Q) and efficiency ($\eta = \frac{J_s}{2\pi}\frac{K_T}{K_Q}$) of the propeller versus advance coefficients (J_s) computed from the analysis program are compared with those given by Brizzolara et al. (2008) in Figure 3. The agreement between the results of the analysis program and those given by Brizzolara et al. (2008) is satisfactory. Therefore, the developed propeller analysis program is validated for the DTMB 4119 propeller. The pressure contours for advance coefficient values, $J_s = 0.6$ and 0.8, are also shown in Figures 4 and 5, respectively, for the completeness of the results.

Note that for this propeller, the pressure contours on all blades and for all blade angles are identical, due to the steady and uniform incoming flow.

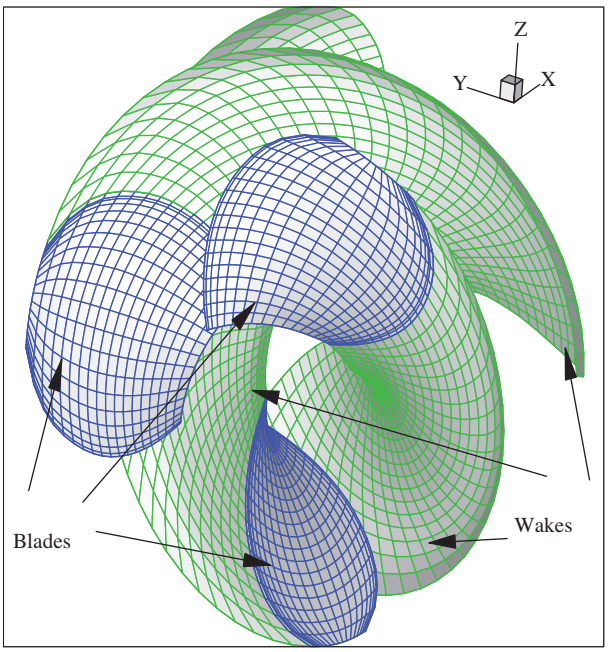

Figure 1. Perspective view of DTMB 4119 propeller blades and wakes.

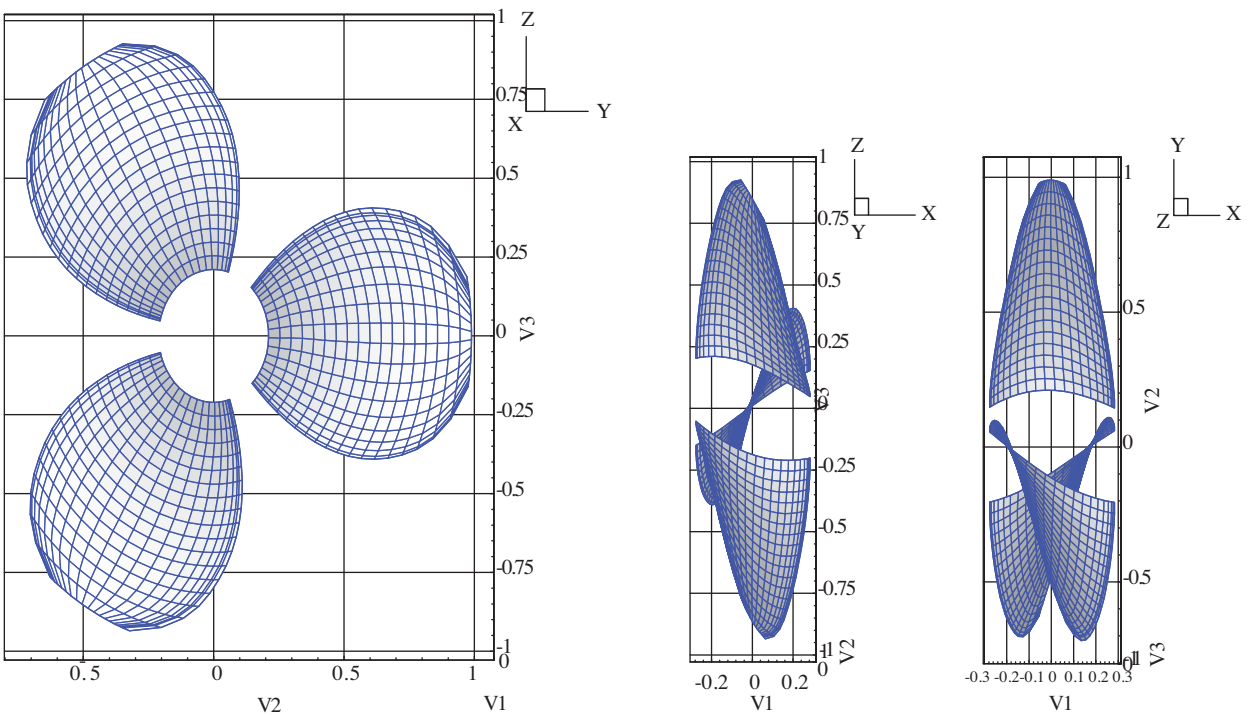

Figure 2. Front and side views of DTMB 4119 propeller and panels used on the blades.

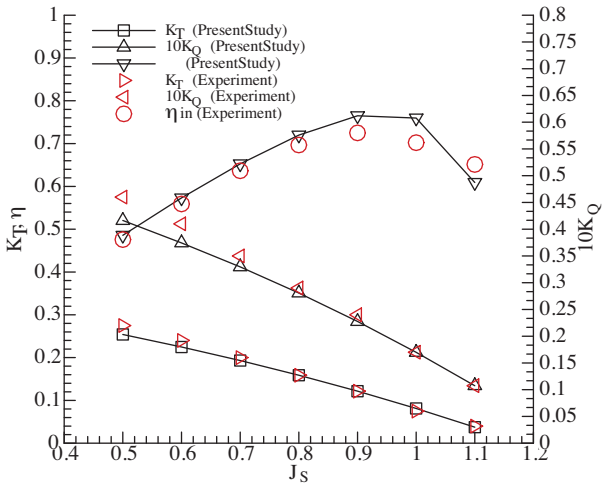

Figure 3. Comparison of K_T, K_Q, and η values with those given by Brizzolara et al. (2008).

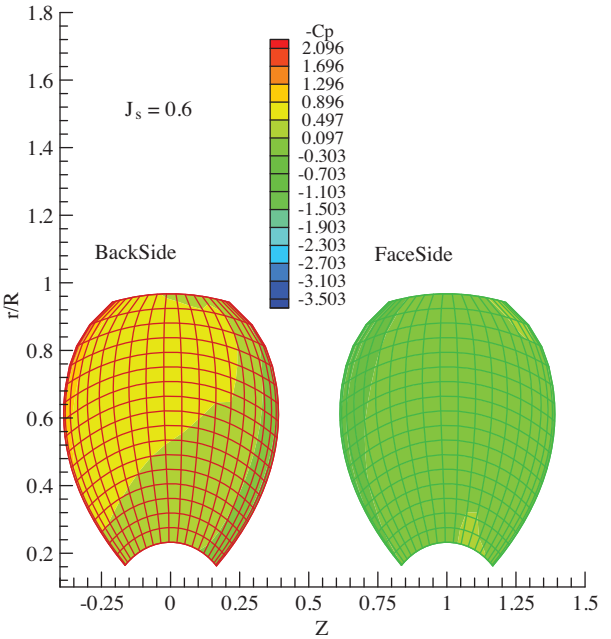

Figure 4. Pressure contours on both sides of blades for noncavitating DTMB 4119 propeller at $J_s = 0.6$.

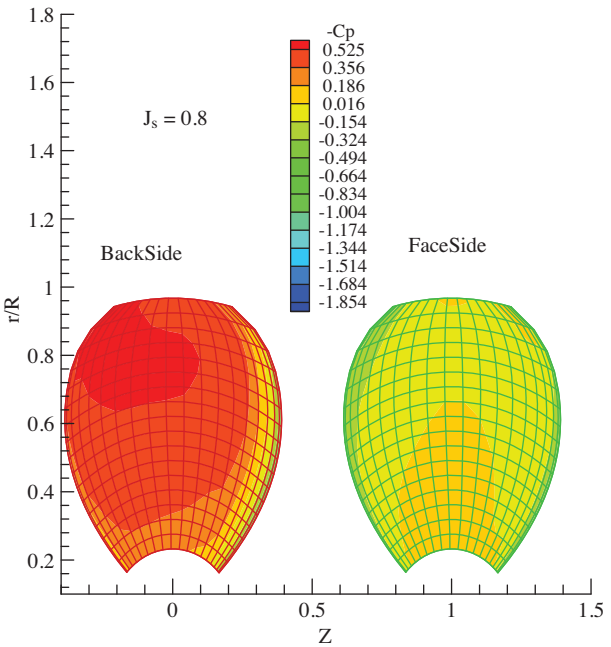

Figure 5. Pressure contours on both sides of blades for noncavitating DTMB 4119 propeller at $J_s = 0.8$.

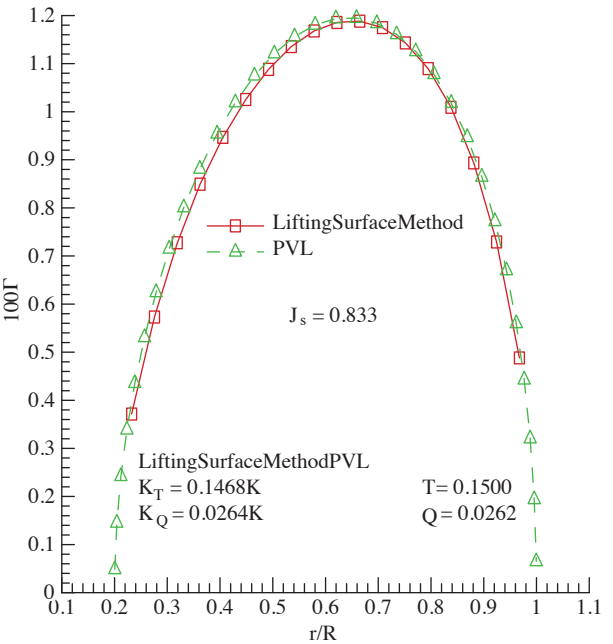

Figure 6. Comparison of circulation distribution with PVL for noncavitating DTMB 4119 propeller.

The design technique was then applied to the DTMB 4119 propeller to check whether or not it is optimum. The advance coefficient (J_s) was assumed to be equal to 0.833 (the design value). The vortex lattice lifting line design program (PVL code given by Kerwin (2001)) was run for the DTMB 4119 propeller at the conditions

given above. The radial optimum circulation distribution, nondimensionalized by $2\pi \mathrm{RV}_R$ (here V_R is the resulting velocity, $V_R = \sqrt{\left(V_S^2 + (0.7D\pi n)^2\right)}$) for design $\mathrm{J}_s = 0.833$, is shown in Figure 6. The thrust and torque coefficients are also included in Figure 6. The lifting surface analysis program was then run to obtain the optimum radial circulation distribution as PVL code. The radial circulation distribution computed from the analysis program (lifting surface method) was compared with those from the PVL code, as shown in Figure 6. The differences between the results of the analysis program and design program are very small. Thus, it can be stated that the blade geometry given in Table 1 for the DTMB 4119 propeller is **almost optimum** under the above design conditions. The thrust and torque coefficients from both the analysis and the design program are also included in Figure 6. Note that the thrust and torque coefficients are also very close to each other. The pressure distributions for 2 different strip numbers (strip numbers 1 and 10) by the propeller analysis program are presented for various advance coefficients in Figures 7 and 8, respectively. Strip 1 corresponds to the blade section at $\mathrm{r} = \mathrm{r}_h$, while strip 10 is very close to the section at $\mathrm{r} = 0.7\mathrm{R}$.

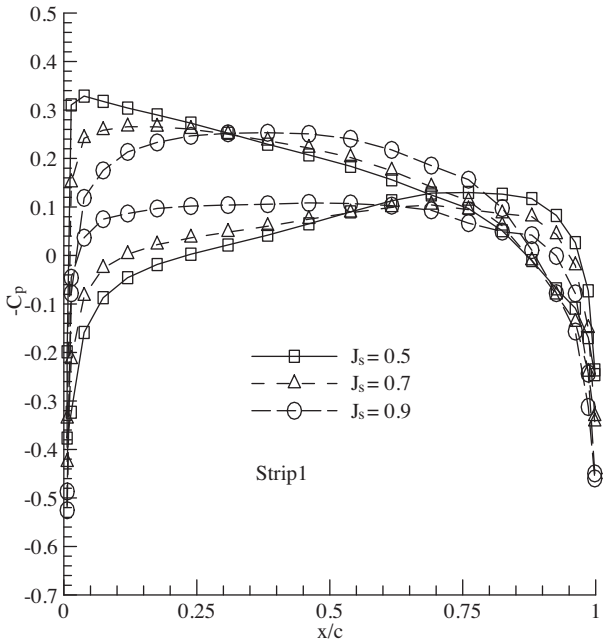

Figure 7. Pressure distribution on strip 1 for different advance coefficients for noncavitating DTMB 4119 propeller.

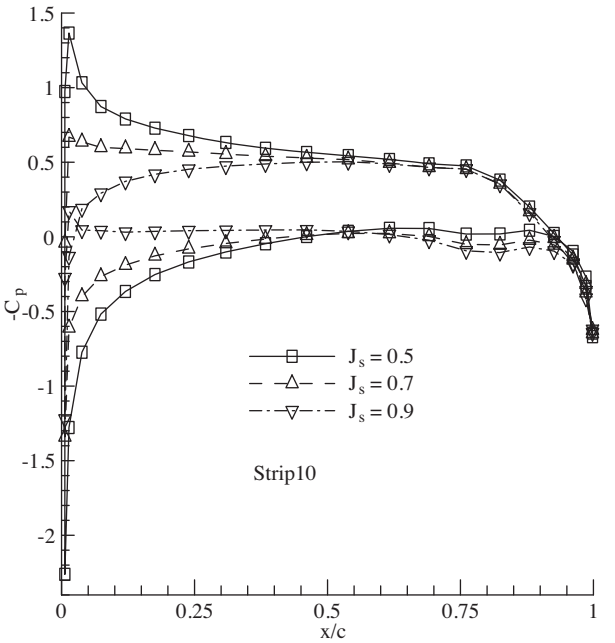

Figure 8. Pressure distribution on strip 10 for different advance coefficients for noncavitating DTMB 4119 propeller.

8.2. Cavitating DTMB 4119 propeller

The design technique was later applied to the same DTMB 4119 propeller with a cavitation number of $\sigma = 1.02$. The working conditions were the same as in the above noncavitating case. There were 20 vortex lattices ($\mathrm{N} = 20$) used along the chordwise direction and 18 vortex lattices ($\mathrm{M} = 18$) used along the radius of the blades. The computed cavity patterns, both on the back and face sides, are shown for design advance coefficient $\mathrm{J}_s = 0.833$ in Figure 9. Note that the cavity occurred only on the back side; there was no cavity on the face side. The radial circulation distribution computed from the analysis program (lifting surface method) is compared

with those from the PVL code in Figure 10. The differences between the results of the analysis program and design program are significantly higher. Thus, it can be stated that the blade geometry given in Table 1 for the original DTMB 4119 propeller with cavitation number $\sigma = 1.02$ is **not optimum** under the above design conditions.

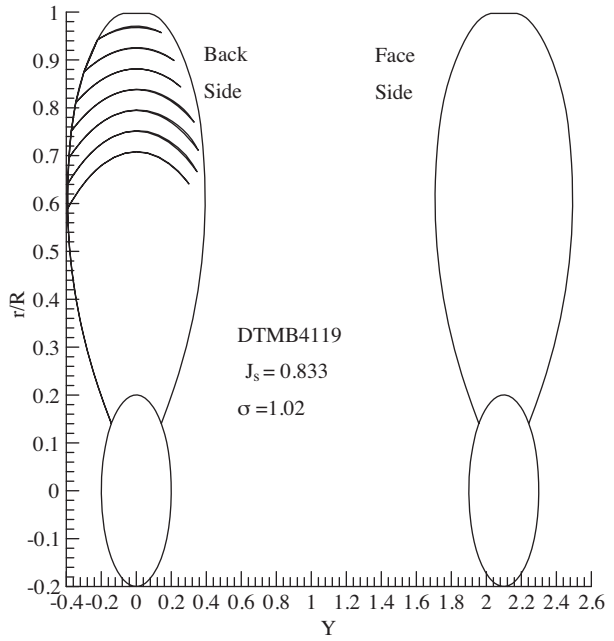

Figure 9. Cavity pattern of original DTMB 4119 propeller for design $J_s = 0.833$ and $\sigma = 1.02$.

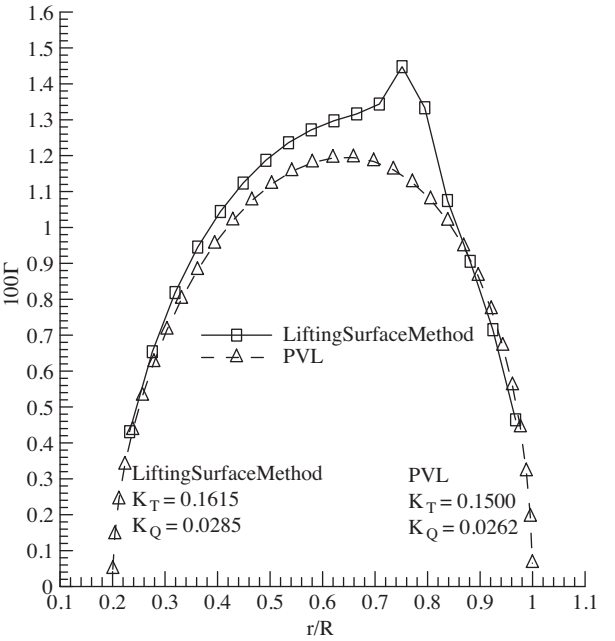

Figure 10. Comparison of circulation distribution with PVL for noncavitating DTMB 4119 propeller.

The code that calls the propeller analysis method (lifting surface solution) repeatedly was then run. This code changes automatically, in a systematic way, the pitch distribution to produce the desired (optimum) circulation distribution for the given chord lengths over the blades. The camber distribution is assumed to be fixed as a first step in this application. The new circulation distribution is given as compared with those from the PVL code in Figure 11. The agreement between the results of the analysis program and design program is very satisfactory. It can be said that the propeller with this new pitch distribution, as given in Figure 12 and as compared with those of the original DTMB 4119 propeller, is **optimum**. Note that the pitch distribution for the original DTMB 4119 propeller decreases from the hub to tip gradually. On the other hand, the pitch distribution for the optimum propeller modified from the DTMB 4119 propeller is constant between r/R = 0.2 and 0.3, then decreases gradually up to r/R = 0.7 and increases faster until the tip of the blade. The thrust and torque coefficients from both the analysis (lifting surface method) and design programs (PVL) are also included in Figure 11. Note also that while the thrust coefficients are very close to each other, the torque coefficients are equal to each other. The cavity patterns for both the original DTMB 4119 propeller and the optimum DTMB 4119 with the new pitch distribution are compared for advance coefficient $J_s = 0.833$ in Figure 13. Both propellers have cavity occurrence on only the back sides of the blades, not on the face sides. The optimum propeller has a smaller cavity formation than the original one.

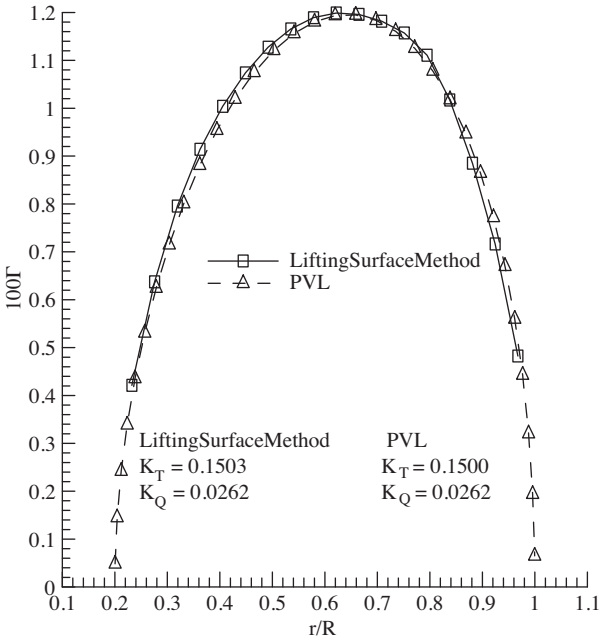

Figure 11. Comparison of circulation distribution with PVL for optimum DTMB 4119 propeller with new pitch distribution.

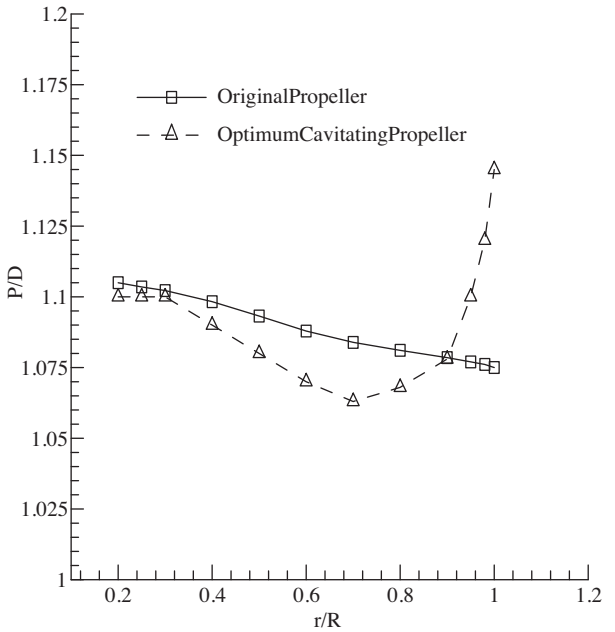

Figure 12. Comparison of new pitch distribution with the original one.

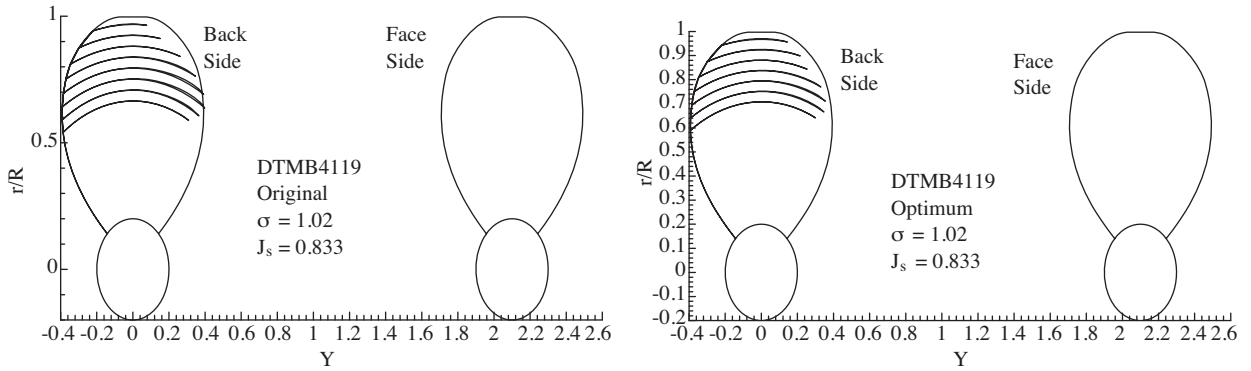

Figure 13. Comparison of cavity pattern of original DTMB 4119 propeller with optimum propeller.

Moreover, the pressure distributions on the optimum propeller for strip number 17 by the propeller analysis program are presented as compared with those of the original DTMB 4119 propeller in Figure 14. Strip number 17 is located very close to the tip and lies under the cavity region on the blade. Note that for the optimum propeller, the cavity length is smaller than that of the original DTMB 4119 propeller. The pressure contours for both the original DTMB 4119 propeller and the optimum propeller are also shown in Figures 15 and 16, respectively, for the completeness of the results. The thrust and torque coefficients (K_T and K_Q) and efficiency (η) of the original DTMB 4119 propeller versus advance coefficients (J_s) computed from the analysis program are compared with those of the optimum propeller in Figure 17. The optimum propeller performance for all of the advance coefficients is slightly better than that of the original DTMB 4119 propeller since the torque coefficients are less than those of the original DTMB 4119 propeller. The cavity formation on both sides of the blades, both for the optimum propeller and the original DTMB 4119 propeller, are also compared for 3

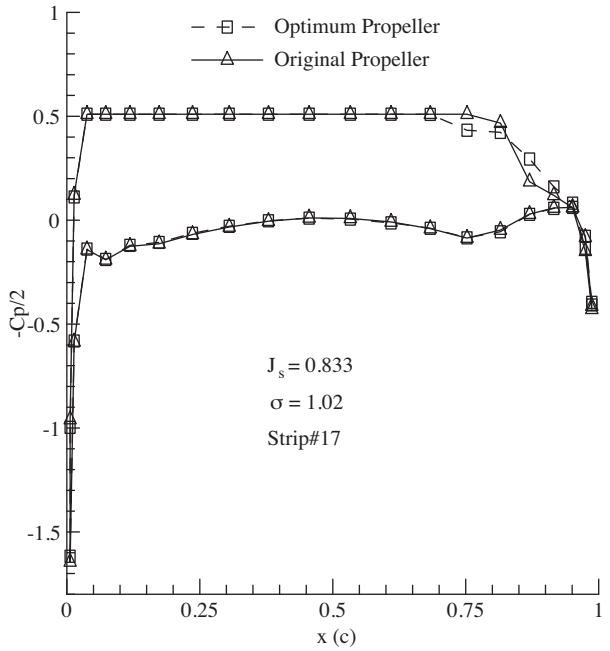

Figure 14. Comparison of pressure distribution of original DTMB 4119 propeller with optimum propeller for J_s = 0.833 and σ = 1.02.

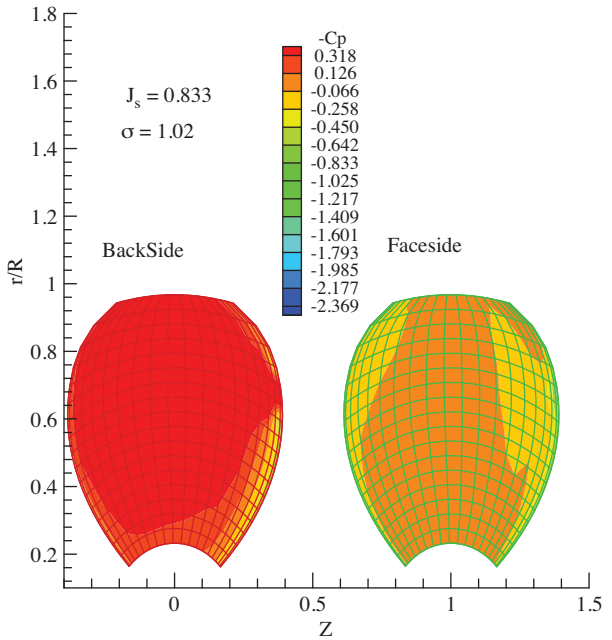

Figure 15. Pressure contours on blades of original DTMB 4119 propeller.

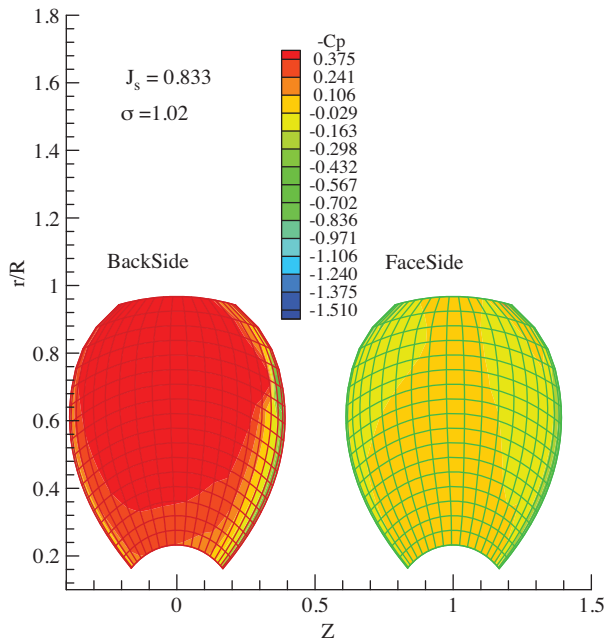

Figure 16. Pressure contours on blades of optimum DTMB 4119 propeller.

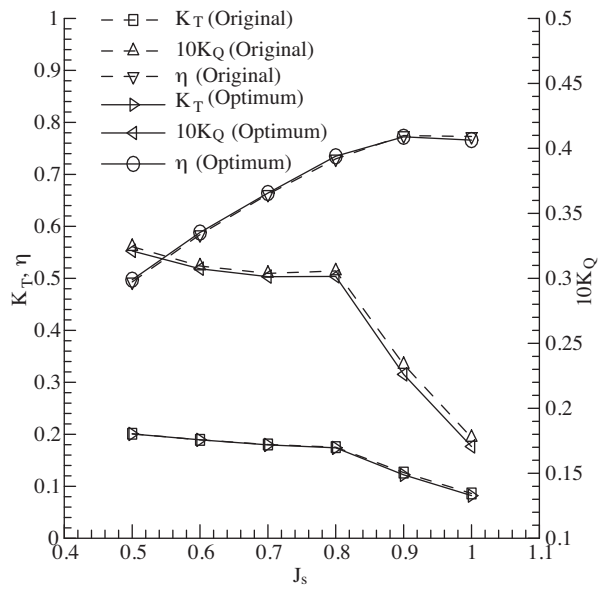

Figure 17. Comparison of K_T, K_Q, and η values of original DTMB 4119 propeller with optimum one.

advance coefficients (J_s = 0.5, 0.7, and 0.9) in Figures 18, 19, and 20, respectively. Note the increasing cavity lengths for decreasing advance coefficients (increasing loading), both for the optimum and the original propeller. Note also the smaller cavity formation for the optimum propeller than for the original propeller for all advance coefficients.

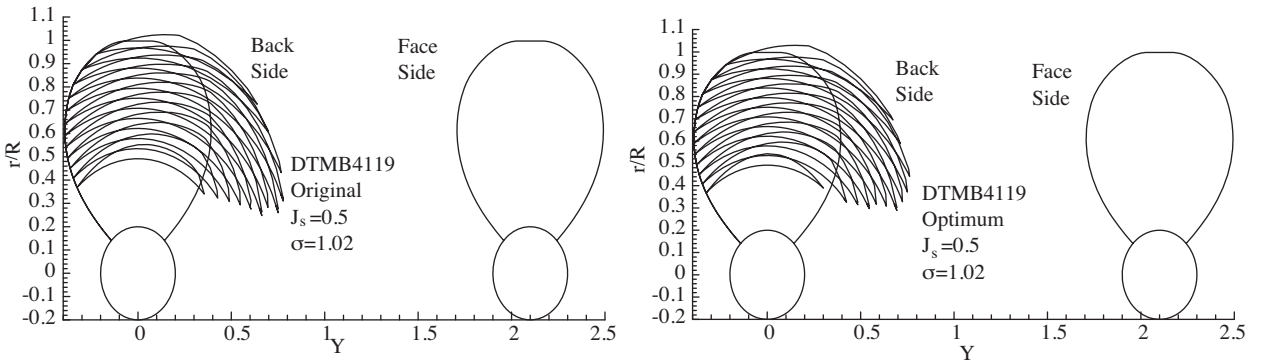

Figure 18. Comparison of cavity pattern of original DTMB 4119 propeller with optimum propeller for J_s = 0.5 and σ = 1.02.

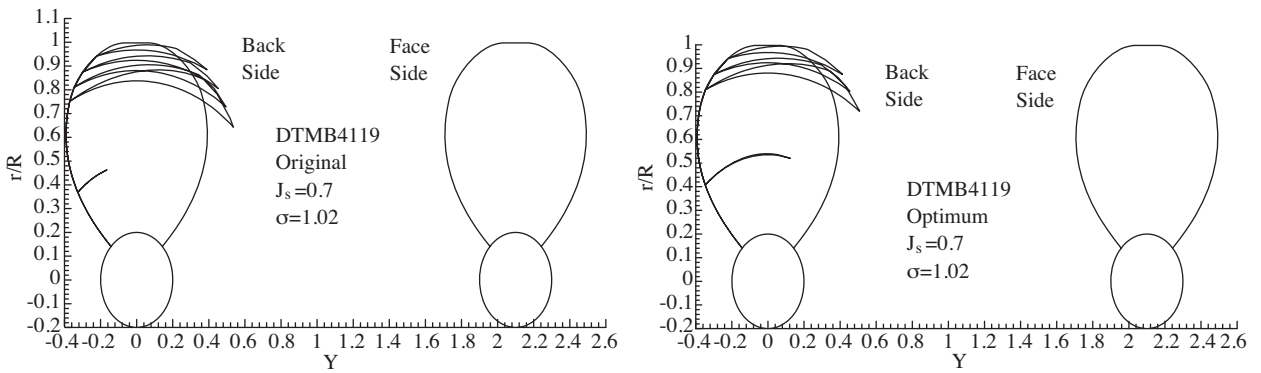

Figure 19. Comparison of cavity pattern of original DTMB 4119 propeller with optimum propeller for J_s = 0.7 and σ = 1.02.

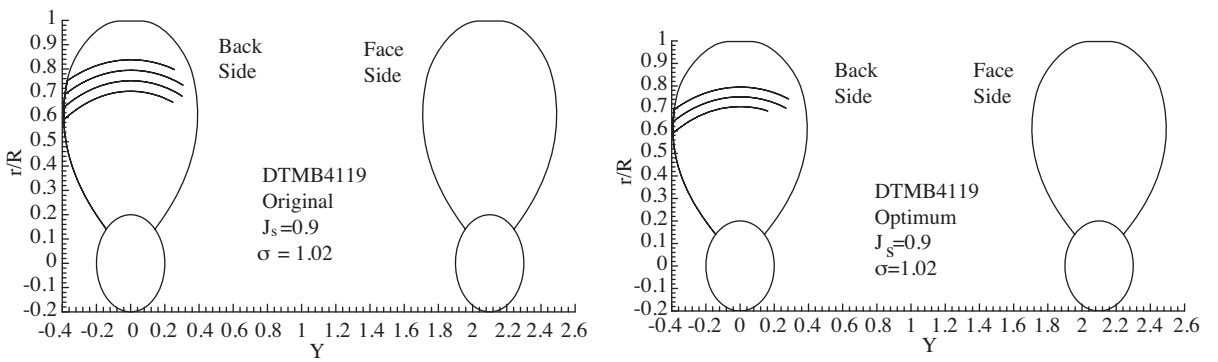

Figure 20. Comparison of cavity pattern of original DTMB 4119 propeller with optimum propeller for J_s = 0.9 and σ = 1.02.

8.3. DTMB 4381 propeller

The design technique was applied to the DTMB 4381 propeller, for which the hydrodynamic characteristics and design conditions were given by Brizzolara et al. (2008). The DTMB 4381 propeller has the following geometric characteristics and working conditions:

i) The propeller is working under uniform inflow.

ii) The propeller has five blades, i.e. NB = 5.

iii) The hub-to-diameter ratio is 0.2.

iv) The cavitation number is 10.

v) The blade geometries from Brizzolara et al. (2008) in terms of radial distribution of the chord length (c), camber (f), thickness (t), and pitch (P) are shown in Table 2.

vi) The blade sections are designed using NACA 66 modified profiles and a camber line of a = 0.8 (refer to Abbott and Doenhoff (1959)).

vii) The propeller has no skew and no rake.

The lifting surface analysis program was run for the DTMB 4381 propeller under the conditions described above. There were 20 vortex lattices used along the chordwise direction and 18 vortex lattices used along the radius of the blades, similar to the case of the DTMB 4119 propeller. The frictional drag coefficient $C_f = 0.0035$ was used in the calculations. The perspective view of the propeller, with its wakes and the vortex elements used in the lifting surface analysis program, is shown in Figure 21. The thrust and torque coefficients and efficiency of the propeller versus advance coefficients (J_s) computed from the analysis program are compared with those of the experiments of Brizzolara et al. (2008) in Figure 22. The agreement between the results of the analysis program and those given by Brizzolara et al. (2008) is satisfactory.

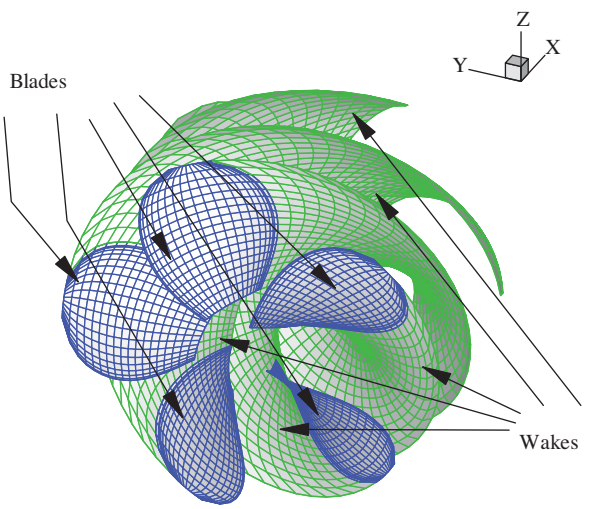

Figure 21. Perspective view of DTMB 4381 propeller blades and wakes.

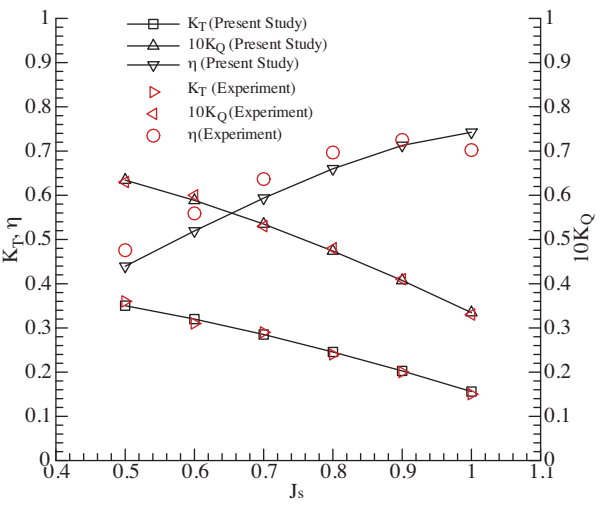

Figure 22. Comparison of K_T, K_Q, and η values with those of experiments by Brizzolara et al. (2008).

Table 2. DTMB 4381 propeller geometry from Brizzolara et al. (2008).

r/R	c/D	P/D	t_{max}/c	f_{max}/c
0.20	0.1740	1.3320	0.2494	0.0351
0.25	0.2020	1.3380	0.1960	0.0369
0.30	0.2290	1.3450	0.1563	0.0368
0.40	0.2750	1.3580	0.1069	0.0348
0.50	0.3120	1.3360	0.0769	0.0307
0.60	0.3370	1.2800	0.0567	0.0245
0.70	0.3470	1.2100	0.0421	0.0191
0.80	0.3340	1.1370	0.0314	0.0148
0.90	0.2800	1.0660	0.0239	0.0123
0.95	0.2100	1.0310	0.0229	0.0128
1.00	0.0010	0.9950	0.0160	0.0123

The vortex lattice lifting line design program was then run for the DTMB 4381 propeller at the conditions given above. The radial optimum circulation distribution for the design $J_s = 0.889$ is shown in Figure 23. The lifting surface analysis program was then run to get the optimum radial circulation distribution for the same chord length distribution as in the PVL code. The radial circulation distribution computed from the analysis program is compared with those from the PVL code in Figure 23. The differences between the results of the analysis program and design program are now significantly higher. Thus, it can be stated that the blade geometry given in Table 2 for DTMB 4381 is **not an optimum** propeller under the above design conditions.

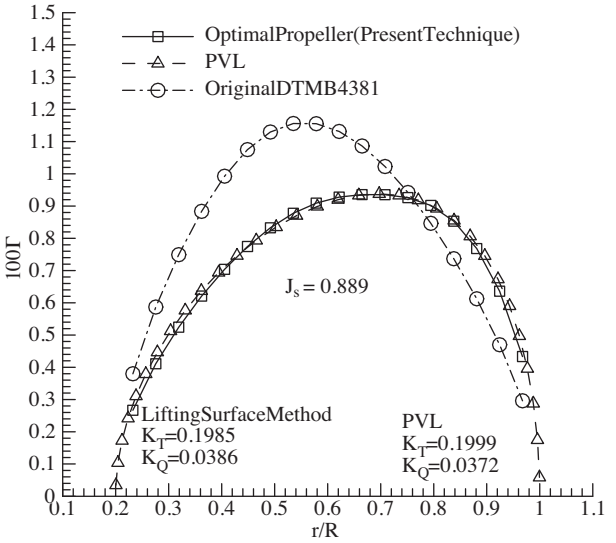

Figure 23. Circulation distribution compared by present design technique and PVL for DTMB 4381 propeller.

The code that calls the propeller analysis method repeatedly was then run. The camber distribution is assumed to be fixed as a first step in this specific application. The new circulation distribution is given, as compared with those of the PVL code, in Figure 23. The agreement between the results of the analysis program and design program is now very satisfactory. It can be said that the propeller with this new pitch distribution, which is given in Figure 24 as compared with that of the original DTMB 4381 propeller, is **optimum**. Note that the pitch distribution for the original DTMB 4381 propeller increases slightly up to $J_s = 0.4$ and then

decreases gradually until the tip of the blade. On the other hand, the pitch distribution for the optimum propeller modified from DTMB 4381 increases up to $J_s = 0.9$ and then decreases until the tip of the blade. Note also that the pitch values are different for both the original and optimum propellers. The thrust and torque coefficients from both the analysis and design programs are included in Figure 13. Note also that the thrust and torque coefficients are very close to each other.

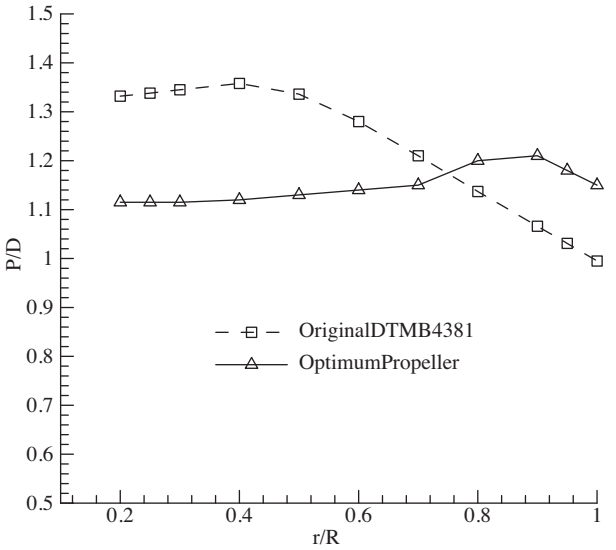

Figure 24. The pitch distribution over blade for both the DTMB 4381 propeller and optimum propeller at design $J_s = 0.889$.

9. Conclusions

A practical design technique for optimum cavitating ship propellers has been described. The hydrodynamic design of a cavitating ship propeller was accomplished in 2 steps, by combining a propeller design method and an analysis method iteratively. The lifting surface analysis method was first validated in the case of a noncavitating DTMB 4119 propeller, for which the geometric and hydrodynamic characteristics are given in the literature. It was found that the agreement between the results (thrust, torque, optimum circulation, and pressure distribution) of the present design technique and those given in the literature is very satisfactory. The design technique was then applied to the same propeller to check whether it is optimum or not, under the given cavity conditions. The method was applied to the DTMB 4381 propeller and the propeller was made optimum under the given working conditions by changing the pitch distribution. It was concluded that:

1. The DTMB 4119 is an optimum propeller in noncavitating conditions. On the other hand, it is not optimum in cavitating working conditions.

2. However, the modified propeller (from the DTMB 4119 propeller) with a new pitch distribution was obtained as optimum while keeping all other geometric characteristics, including pitch, camber, and chord, fixed.

3. The technique is very fast and effective and can be used as a reliable tool for many practical applications. Refer to Bal (2011a) for the other practical applications of the present lifting surface method to noncavi-

tating propellers. Refer also to Bal (2011b) for applications of the present method to different cavitating propellers.

Nomenclature

a	NACA camber (mean) line constant
c(r)	chord length along blade
C_f	frictional drag coefficient
$C_p(P_i)$	pressure coefficient
d	distance between vortex element and field point
D	propeller diameter
f	camber parameter for blade section
f_{max}	maximum camber of each blade section
J_s	advance coefficient = $V_s/(nD)$
NB	number of blades
K_T	thrust coefficient of propeller = $T/(\rho n^2 D^4)$
K_Q	torque coefficient of propeller = $Q/(\rho n^2 D^5)$
M	number of radial vortex lattice elements
n	propeller rotational speed [rps]
$\vec{n}_m$	unit vector normal to the mean camber or trailing wake surface
p	pressure
P(r)	pitch of blade section
Q	propeller torque
r_h	radius of hub
PVL	propeller vortex lattice code
R	radius of propeller
t	thickness parameter for blade sections
t_{max}	maximum thickness of each blade section
T	propeller thrust
$u_a^*(r)$	axial induced velocity along blade
$u_t^*(r)$	tangential induced velocity along blade
x, r, θ	cylindrical coordinates rotating with blade
V_a	effective axial inflow
V_R	resulting velocity = $\sqrt{\left(V_S^2 + (0.7D\pi n)^2\right)}$
V_S	uniform incoming flow velocity
V_t	effective tangential inflow
$\vec{v}_\Gamma$	velocity vector induced by each unit strength vortex element
$\vec{v}_Q$	velocity vector induced by each unit strength source element
w_x r	axial wake fraction
β(r)	pitch angle of blade section
η	propeller efficiency = $J_s/(2\pi)K_T/K_Q$
Γ	circulation
ω	angular velocity = $2\pi n$
ρ	density of water

References

Abbott, I.H. and von Doenhoff, A.E., The Theory of Wing Sections, Dover Inc., New York, NY, USA, 1959.

Bal, S., "A Practical Technique for Improvement of Open Water Propeller Performance", Proceedings of the Institution of Mechanical Engineers, Part M, Journal of Engineering for the Maritime Environment, DOI 10.1177/1475090 211 413957, in print,, 2011a.

Bal, S., "Computation of Optimum Cavitating Ship Propellers", Journal of Naval Architecture and Marine Technology, The Turkish Chamber of Naval Architects and Marine Engineers, 187, 29-33, 2011b (in Turkish).

Bal, S. and Güner, M., "Performance Analysis of Podded Propulsors", Ocean Engineering, 36, 556-563, 2009.

Betz, A., "Schraubenpropeller mit Geringstem Energieverlust", K. Ges. Wiss. Gottingen Nachr. Math.-Phys. Klasse, 193-217, 1919.

Breslin, J.P. and Andersen, P., Hydrodynamics of Ship Propellers, Cambridge University Press, UK, 1994.

Brizzolara, S., Villa, D. and Gaggero, S., "A Systematic Comparison Between RANS and Panel Methods for Propeller Analysis", Proc. of 8th International Conference on Hydrodynamics, Nantes, France, Sep. 30-Oct. 3, 2008.

Coney, W.B., "Optimum Circulation Distributions for a Class of Marine Propulsors", Journal of Ship Research, 36, 210-222, 1992.

Dai, C., Hambric, S., Mulvihill, L., Tong, S.S. and Powell, D., "A Prototype Marine Propulsor Design Tool Using Artificial Intelligence and Numerical Optimization Techniques", Trans. SNAME, 102, 57-69, 1994.

Goldstein, S., "On the Vortex Theory of Screw Propellers", Proc. Royal Soc. London, Series A, 123, 440-465, 1929.

Greely, D.S. and Kerwin, J.E., "Numerical Methods for Propeller Design and Analysis in Steady Flow", Trans. SNAME, 90, 415-453, 1982.

Griffin, P.E. and Kinnas, S.A., "A Design Method for High-Speed Propulsor Blades", Journal of Fluids Engineering, 120, 556-562, 1998.

Kerwin, J.E., "Marine Propellers", Annual Review of Fluid Mechanics, 18, 367-403, 1986.

Kerwin, J.E., "Hydrofoils and Propellers", Lecture Notes, Department of Ocean Engineering, Massachusetts Institute of Technology, USA, January 2001.

Kerwin, J.E., "The Preliminary Design of Advanced Propulsors", Proc. of Propellers/Shafting 2003 Symposium, SNAME, Virginia Beach, VA, USA, September 16-17, 2003.

Kerwin, J.E. and Lee, C.S., "Prediction of Steady and Unsteady Marine Propeller Performance by Numerical Lifting-Surface Theory", Trans. SNAME, 86, 218-253, 1978.

Kinnas, S.A., Lee, H.S., Gu, H., and Deng, Y., "Prediction of Performance and Design via Optimization of Ducted Propellers Subject to Non-Axisymmetric Inflows", Trans. SNAME, 113, 99-121, 2005.

Kuiper, G. and Jessup, S.D., "A Propeller Design Method for Unsteady Conditions", Trans. SNAME, 101, 247-273, 1993.

Lerbs, H.W., "Moderately Loaded Propellers with a Finite Number of Blades and Arbitrary Distribution of Circulation", Trans. SNAME, 60, 73-117, 1952.

Mishima, S. and Kinnas, S.A., "Application of a Numerical Optimization Technique to the Design of Cavitating Propellers in Non-Uniform Flow", Journal of Ship Research, 41, 93-107, 1997.

Sparenberg, J.A., "On Optimum Propellers with a Duct of Finite Lengths", Journal of Ship Research, 13, 129-136, 1969.

Sun, H., Performance Prediction of Cavitating Propulsors Using a Viscous/Inviscid Interaction Method, PhD Thesis, Ocean Engineering Group, The University of Texas at Austin, USA, 2008.